CORA Cork Open Research Archive
Cartlann Taighde Oscailte Chorcaí

Title	Alkali-carbonate melts in the cratonic mantle evidenced by a wehrlite xenolith from the Majuagaa kimberlite, West Greenland
Authors	Kiseeva, Ekaterina S.;Kamenetsky, Vadim S.;Chayka, Ivan F.;Maas, Roland;Nielsen, Troels F. D.
Publication date	2024-10-09
Original Citation	Kiseeva, E. S., Kamenetsky, V. S., Chayka, I. F., Maas, R. and Nielsen, T. F. D. (2024) 'Alkali-carbonate melts in the cratonic mantle evidenced by a wehrlite xenolith from the Majuagaa kimberlite, West Greenland', Geology, 53(1), pp.89-93. https://doi.org/10.1130/G52274.1
Type of publication	Article (peer-reviewed)
Link to publisher's version	10.1130/g52274.1
Rights	© 2024, the Authors. Gold Open Access: This paper is published under the terms of the CC-BY license. - https://creativecommons.org/licenses/by/4.0/
Download date	2026-11-04 17:13:37
Item downloaded from	https://hdl.handle.net/10468/16571

UCC
University College Cork, Ireland
Coláiste na hOllscoile Corcaigh

Kiseeva, E.S., et al., 2024, Alkali-carbonate melts in the cratonic mantle evidenced by a wehrlite xenolith from the Majuagaa kimberlite, West Greenland: Geology, v. XX, p. XXX–XXX, https://doi.org/10.1130/G52274.1

Supplemental Material

Description of the Rb-Sr and Sm-Nd isotopic analyses and results, Table S1, Figures S1–S6, and additional references.

Supplemental Material

Alkali-carbonate melts in the cratonic mantle evidenced by a wehrlite xenolith from the Majuagaa kimberlite, West Greenland

Ekaterina S. Kiseeva, Vadim S. Kamenetsky, Ivan F. Chayka, Roland Maas, Troels F. D. Nielsen

Rb-Sr and Sm-Nd isotope results

In an effort to trace the source of inferred carbonatitic veining in wehrlite xenolith GGU473178, Rb-Sr and Sm-Nd isotope data were acquired for two samples from the xenolith: a clinopyroxene separate and a 'carbonate' fraction extracted from chips of the veined xenolith material (GK1xCPX, GK1xL). For comparison, isotopic data were also acquired for an ilmenite/perovskite concentrate in a sample of the host kimberlite (GL1ILM). Finally, a whole rock powder of the host kimberlite was sequentially leached with water and dilute HCl to extract easily soluble components (GK1xL1, GK1xL2). The HCl leachate is assumed to have mobilized carbonate minerals within the kimberlite.

1. Methods

All sample preparation and analytical work was carried out at the University of Melbourne (e.g. Dalton et al., 2020; Maas et al., 2022; Woodhead et al., 2019). To produce a carbonate fraction from the wehrlite xenolith, mm-sized fragments of the xenolith (ca. 1 g) were reacted with 2M HCl-HNO_3 (12 hrs, 60°C) to preferentially dissolve the carbonate-rich vein material. This solution and a distilled water rinse of the resulting residue was transferred to a separate beaker (sample GK1xL); the mass removed during the leaching was estimated to be ~0.02 g. A broadly similar treatment was used for the host kimberlite: whole rock powder (GK1, 0.088 g) was reacted with distilled water (40°C, 1 hr) to release easily soluble compounds (e.g., chlorides); the water leachate (GK1 L1) was removed and stored. The residue was reacted with 2M HCl (60°C, 1 hr) and the solution removed, combined with another distilled water rinse, and stored (GK1 L2). Sample mass in GK1 L1 and L2 was estimated to be 3 and 5%, respectively, leaving 80.8 mg of residue. This residue (GK1R), assumed to be mainly silicates and oxides, was dissolved at high pressure in HF-HNO_3 and HNO_3 (24 hrs each, 120°C). In addition to these leach fractions, a clinopyroxene concentrate (GK1xCPX, 17.6 mg) from the wehrlite xenolith matrix and an ilmenite/perovskite separate (GK1 ILM, 5.01 mg) from the host kimberlite were cleaned with dilute HNO_3 and dissolved in HF-HNO_3 and HNO_3 at low pressure (120°C, 48 hrs).

Following determination of approximate Rb-Sr-Nd concentrations, all or part of the sample solutions were equilibrated with ^{85}Rb-^{84}Sr and ^{149}Sm-^{150}Nd spike solutions; GK1 L1 was only spiked with the Rb-Sr tracer because Nd contents were too low for analysis. Elemental extractions for Sr and Rb were done on small columns of Eichrom Sr resin (50-100 μm) and 4ml columns of AG50-X8 (200-400 mesh) cation resin, respectively; 2 passes over the Sr resin were done to produce clean Sr fractions. Samarium and Nd were extracted and separated using Eichrom TRU- and LN-resins (Pin et al., 2014). Procedural blanks were ≤0.05 ng and negligible.

Isotopic analyses were carried out on a Nu Instruments Plasma 1 multi-collector ICP-MS, with sample introduction via a low-uptake Glass Expansion PFA nebuliser and

CETAC Aridus desolvation system. Strontium isotope data were acquired on signals of 8-10V total Sr, corrected for Kr, Sr memory, Rb interference and spike impurities, and normalized to $^{88}Sr/^{86}Sr=8.37521$, using the exponential law as part of an online, iterative spike unmixing/mass bias correction procedure. Internal precision (2se) for $^{87}Sr/^{86}Sr$ is typically ±0.000020 or less while external precision is near ±0.000040 (2sd). $^{84}Sr/^{86}Sr$ in unspiked Sr averages 0.05648±3 and $^{87}Sr/^{86}Sr$ for SRM987 averaged 0.71019 during this campaign; final $^{87}Sr/^{86}Sr$ data for secondary standards and unknowns are reported relative to SRM987=0.71023. Rb isotopic analyses were done using Zr-doping (Waight et al., 2002) and external precision for $^{87}Rb/^{86}Sr$ determined by isotope dilution is ±0.5% (2sd). Neodymium isotope data were acquired with signals of 15-20V total Nd, corrected for Sm interference and spike impurities, and internally normalized to $^{146}Nd/^{145}Nd = 2.0719425$ (equivalent to the more familiar $^{146}Nd/^{144}Nd = 0.7219$, Vance and Thirlwall, 2002) as part of an online iterative spike unmixing/mass bias correction procedure. Internal precision (2se) for $^{143}Nd/^{144}Nd$ is typically ±0.000008-0.000015 while external precision is estimated to be near ±0.000020 (2sd); results for $^{143}Nd/^{144}Nd$ are reported relative to La Jolla Nd = 0.511860. The $^{147}Sm/^{144}Nd$ ratio determined by isotope dilution has an external precision of ±0.2% (2sd). A modern chondritic (CHUR) composition of $^{147}Sm/^{144}Nd=0.1960$ and $^{143}Nd/^{144}Nd=0.512630$ was used to calculate ε_{Nd} values (Bouvier et al., 2008). The decay constants are: ^{87}Rb $1.397x10^{-11}$/yr, ^{147}Sm $6.54x10^{-12}$/yr.

USGS basalt BCR-2 processed with the unknowns yielded $^{87}Sr/^{86}Sr = 0.704973±20$ and $^{143}Nd/^{144}Nd = 0.512630±7$, 0.512634±10 and 0.512634±9, while USGS basalt BHVO-2 produced 0.703434±14, 0.703454±13 and 0.512997±11. Isotope dilution analyses of four spiked splits of a single digestion of BCR-2 basalt averaged 45.90±0.01 ppm Rb, 333.8±0.2 ppm Sr, $^{87}Rb/^{86}Sr$ 0.3976±0.0003 and $^{87}Sr/^{86}Sr$ 0.704979±0.000017 (2sd). A compilation of 26 Sm-Nd isotope dilution analyses for this standard yields averages of 6.43±0.08 ppm Sm, 28.09±0.28 ppm Nd, $^{147}Sm/^{144}Nd$ 0.1382±0.0003 and $^{143}Nd/^{144}Nd$ 0.512639±0.000024 (all 2sd). These results are consistent with reference data (e.g., GeoREM, http://georem.mpch-mainz.gwdg.de).

2. Results

The Rb-Sr compositions for the clinopyroxene and the carbonate fraction (assumed to be dominated by the carbonatitic vein material) from wehrlite xenolith GGU473178 are similar, with $^{87}Rb/^{86}Sr$ and $^{87}Sr/^{86}Sr$ of 0.223/0.70428 and 0.106/0.70419, respectively (Table SM1). The large differences in Sr contents (177 vs 1119 ppm) may be related in part to uncertainty in the weight of the GK1xL fraction. This would also affect the calculated Nd and Sm concentrations which are much higher (72.3 ppm, 9.0 ppm) in GK1xL than in GK1xCPX (6.9 ppm, 1.6 ppm). Measured $^{147}Sm/^{144}Nd$ ratios contrast strongly (Table SM1) and provide an apparent 2-point age of 595 Ma, broadly consistent with the emplacement age of the host kimberlite (ca. 560 Ma, Tappe et al., 2011). Age-correction to 560 Ma yields indistinguishable ε_{Ndi} (+3.5 and +3.2) but $^{87}Sr/^{86}Sr_i$ is lower in the clinopyroxene (0.70253) than in the carbonate fraction (0.70336).

Ilmenite/perovskite from the host kimberlite (GK1ILM) has 23.6 ppm Sr, 131 ppm Nd (implying a low perovskite content) and age-corrected $^{87}Sr/^{86}Sr$-ε_{Nd} of 0.70314 and +2.8; this isotopic signature is consistent with the kimberlite's classification as a Group

1/archetypal kimberlite. Strontium concentrations in the leachate (GK1L1-GK1L2) and residue (GK1R) fractions (119, 3403 and 53 ppm) for the host kimberlite are diverse, but, as noted for GK1xL, elemental concentrations in the two leachates may be affected by uncertainty in sample weights. In a Rb-Sr isochron diagram, the compositions of GK1xL1, GK1xL2 and GK1xR define a straight line with an apparent age of 551±68 Ma (MSWD 5, $^{87}Sr/^{86}Sr_i$ 0.70423±47), indistinguishable from the 560 Ma kimberlite emplacement age. The Sm/Nd ratios in GK1L2 and GK1R (GK1L1 was not analysed) are low ($^{147}Sm/^{144}Nd$ <0.08), and age-corrected ε_{Nd} values are +3.0 and +3.3, respectively (Table SM1).

3. Conclusions

The wehrlite xenolith and its kimberlite host rock show homogeneous initial ε_{Nd} (+2.8 to +3.5) but substantial range in initial $^{87}Sr/^{86}Sr$ (0.7025-0.7042), replicating the isotopic range found in Majuagaa Kimberlite by Tappe et al. (2011). The Rb-Sr isotopic systematics in the host kimberlite appear to be primary, cf. the match between a 551 Ma Rb-Sr age for leachate-residue fractions to the perovskite-based emplacement age for the kimberlite. Importantly, this age match suggests a close genetic link of the carbonate component and the kimberlite. The apparent Sm-Nd age of 595 Ma defined by clinopyroxene and a carbonate component in the wehrlite xenolith supports wehrlitization of local peridotite during the Neoproterozoic kimberlite event.

References

Bouvier, A., Vervoort, J. D., and Patchett, P. J., 2008, The Lu–Hf and Sm–Nd isotopic composition of CHUR: constraints from unequilibrated chondrites and implications for the bulk composition of terrestrial planets: Earth and Planetary Science Letters, v. 273, no. 1-2, p. 48-57.

Dalton, H., Giuliani, A., Phillips, D., Hergt, J., Maas, R., Matchan, E., Woodhead, J., and O'Brien, H., 2020, A comparison of geochronological methods commonly applied to kimberlites and related rocks: Three case studies from Finland: Chemical Geology, v. 558, p. 119899.

Maas, R., Apukhtina, O. B., Kamenetsky, V. S., Ehrig, K., Sprung, P., and Münker, C., 2022, Carbonates at the supergiant Olympic Dam Cu-U-Au-Ag deposit, South Australia part 2: Sm-Nd, Lu-Hf and Sr-Pb isotope constraints on the chronology of carbonate deposition: Ore Geology Reviews, v. 140, p. 103745.

Pin, C., Gannoun, A., and Dupont, A., 2014, Rapid, simultaneous separation of Sr, Pb, and Nd by extraction chromatography prior to isotope ratios determination by TIMS and MC-ICP-MS: Journal of Analytical Atomic Spectrometry, v. 29, no. 10, p. 1858-1870.

Tappe, S., Pearson, D. G., Nowell, G., Nielsen, T., Milstead, P., and Muehlenbachs, K., 2011, A fresh isotopic look at Greenland kimberlites: cratonic mantle lithosphere imprint on deep source signal: Earth and Planetary Science Letters, v. 305, no. 1, p. 235-248.

Vance, D., and Thirlwall, M., 2002, An assessment of mass discrimination in MC-ICPMS using Nd isotopes: Chemical Geology, v. 185, no. 3-4, p. 227-240.

Waight, T., Baker, J., and Willigers, B., 2002, Rb isotope dilution analyses by MC-ICPMS using Zr to correct for mass fractionation: towards improved Rb–Sr geochronology ? : Chemical Geology, v. 186, no. 1-2, p. 99-116.

Woodhead, J., Hergt, J., Giuliani, A., Maas, R., Phillips, D., Pearson, D. G., and Nowell, G., 2019, Kimberlites reveal 2.5-billion-year evolution of a deep, isolated mantle reservoir: Nature, v. 573, no. 7775, p. 578-581.

Alkali-carbonate melts in the cratonic mantle evidenced by a wehrlite xenolith from the Majuagaa kimberlite, West Greenland

Ekaterina S. Kiseeva, Vadim S. Kamenetsky, Ivan F. Chayka, Roland Maas, Troels F. D. Nielsen

Table S1 **Rb-Sr and Sm-Nd isotope compositions for Majuagaa Kimberlite and GGU473178 xenolith**

	host kimberlite				xenolith	
code	GK1 ILM	GK1 L1	GK1 L2	GK1 R	GK1xCPX	GK1xL
	ilmenite	water leach	acid leach	residue	clinopyroxene	carbonate
Rb ppm*	1.89	7.76	95.17	19.82	13.67	40.88
Sr ppm*	23.63	119.4	3403	52.74	177.3	1119
$^{87}Rb/^{86}Sr$	0.2319	0.1879	0.0809	1.087	0.2230	0.1056
$^{87}Sr/^{86}Sr$	0.704963	0.705716	0.704826	0.712626	0.704275	0.704185
±2se	0.000015	0.000017	0.000017	0.000015	0.000016	0.000015
Sm ppm*	15.63		22.58	3.47	1.63	9.02
Nd ppm*	131.6		173.3	28.74	6.86	72.28
$^{147}Sm/^{144}Nd$	0.0717		0.0787	0.0728	0.1438	0.0753
$^{143}Nd/^{144}Nd$	0.512319		0.512353	0.512345	0.512617	0.512349
±2se	0.000010		0.000009	0.000009	0.000012	0.000009
$^{87}Sr/^{86}Sr$ @ 560 Ma	0.70314	0.70424	0.70419	0.70410	0.70253	0.70336
ε_{Nd} @ 560 Ma	2.8		3.0	3.3	3.5	3.2

*despite being the result of high-precision isotope dilution analyses, the elemental concentrations in leachates GK1 L1, GK1 L2 and GK1xL
are uncertain because sample weights were estimated rather than measured

For further details, see main text of Supplemental Material

Alkali-carbonate melts in the cratonic mantle evidenced by a wehrlite xenolith from the Majuagaa kimberlite, West Greenland

Ekaterina S. Kiseeva, Vadim S. Kamenetsky, Ivan F. Chayka, Roland Maas, Troels F. D. Nielsen

Figure S1. From Pilbeam et al., 2023. Map of southern West Greenland showing the location of the Majuagaa kimberlite dyke in the Maniitsoq region

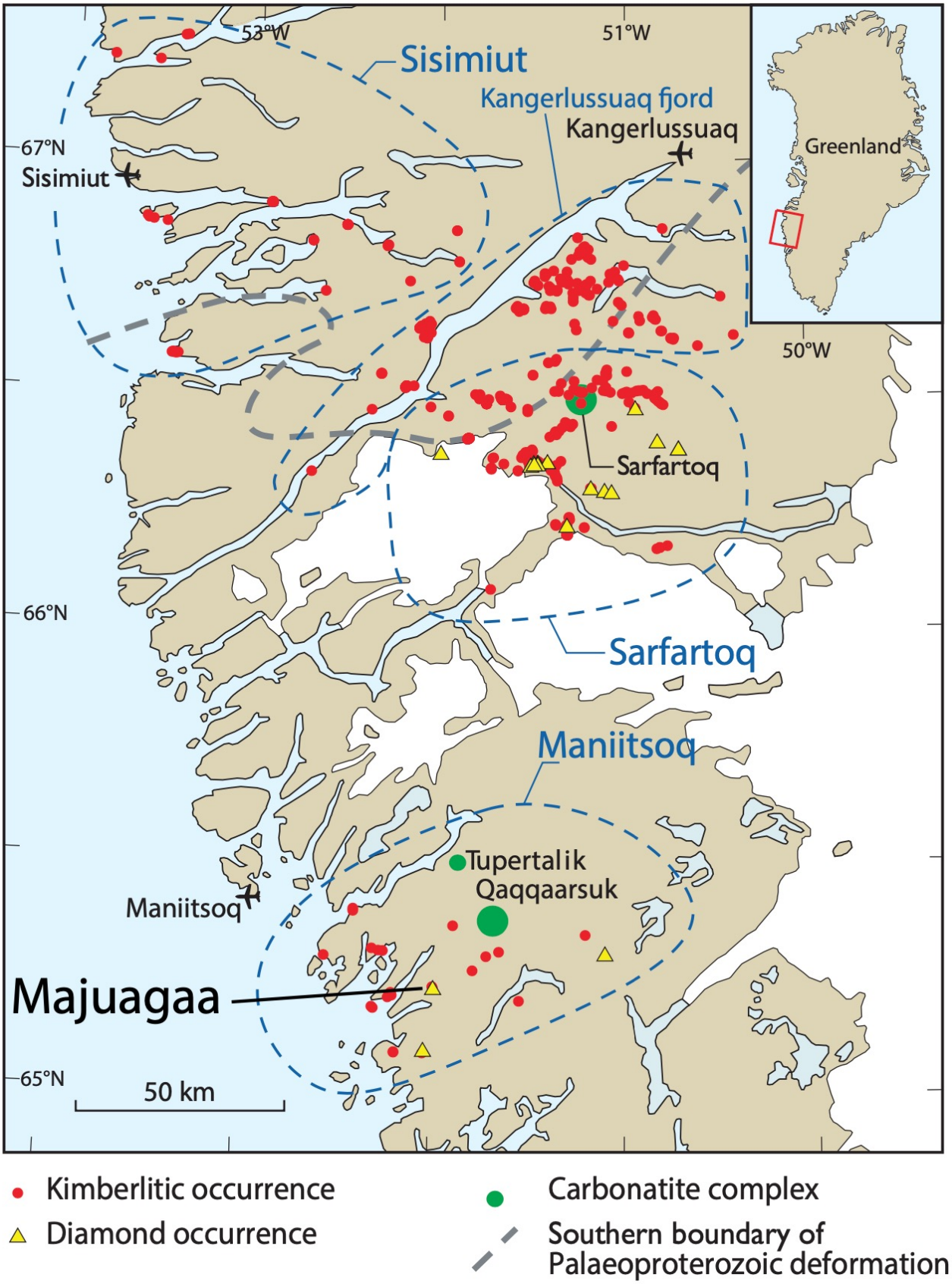


Figure S2. CaO-Cr_2O_3 diagram of garnet compositions after Sobolev et al. 1973. Plotted data show garnet compositions from wehrlites sourced from Georock database with wehrlites identified by the source literature. Three garnet compositions from West Greenland were reported for wehrlites by Sand et al. 2009.

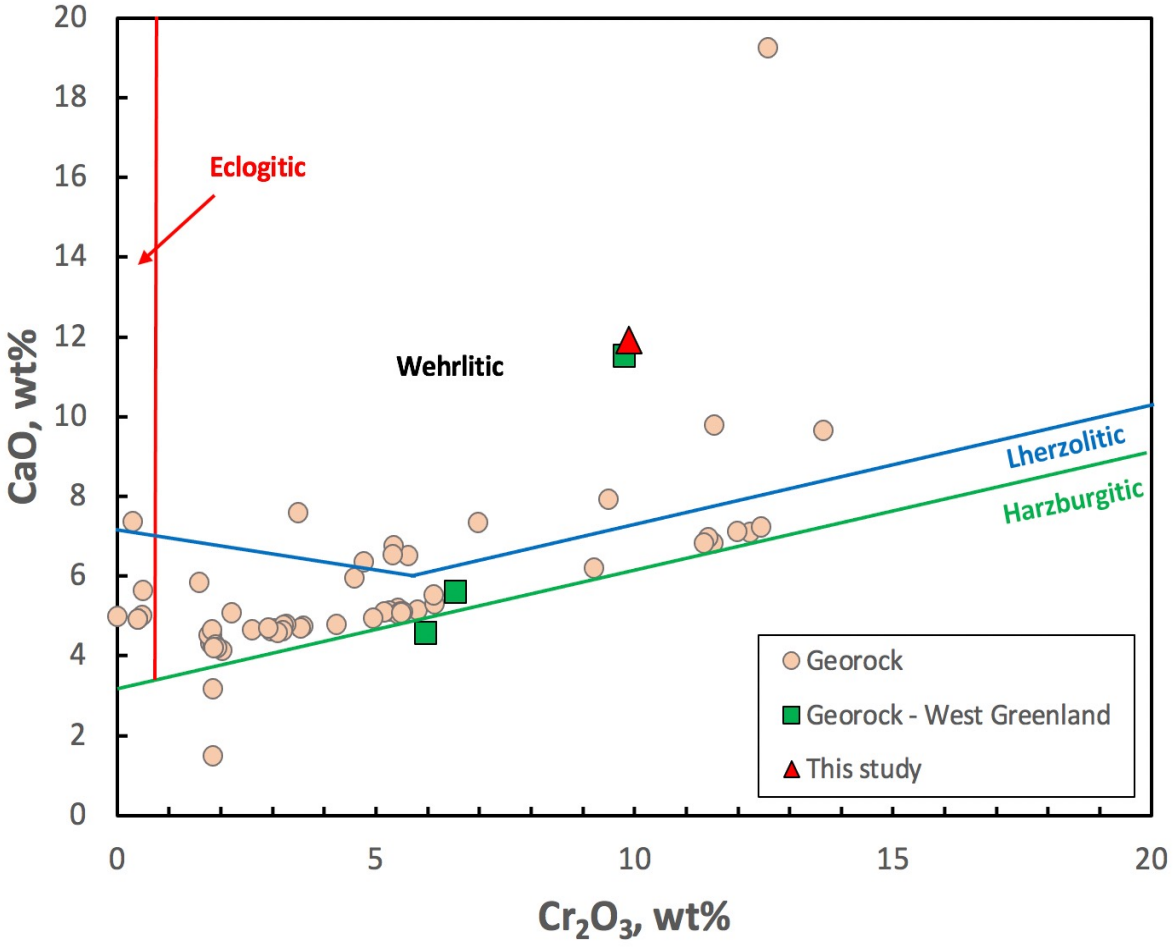


Figure S3. Melt pools composed of predominantly dolomite, subordinate calcite and serpentine. Serpentine is rimmed by Fe-oxides in ocelli. Also present Na- and Sr-rich apatite, spinel, phlogopite/tetraferriphlogopite, minor Fe-Ni sulfides, djerfisherite, alkali carbonates, Sr-Ba carbonates, Sr-La-Ce sulfates, K-Na chlorides and barite

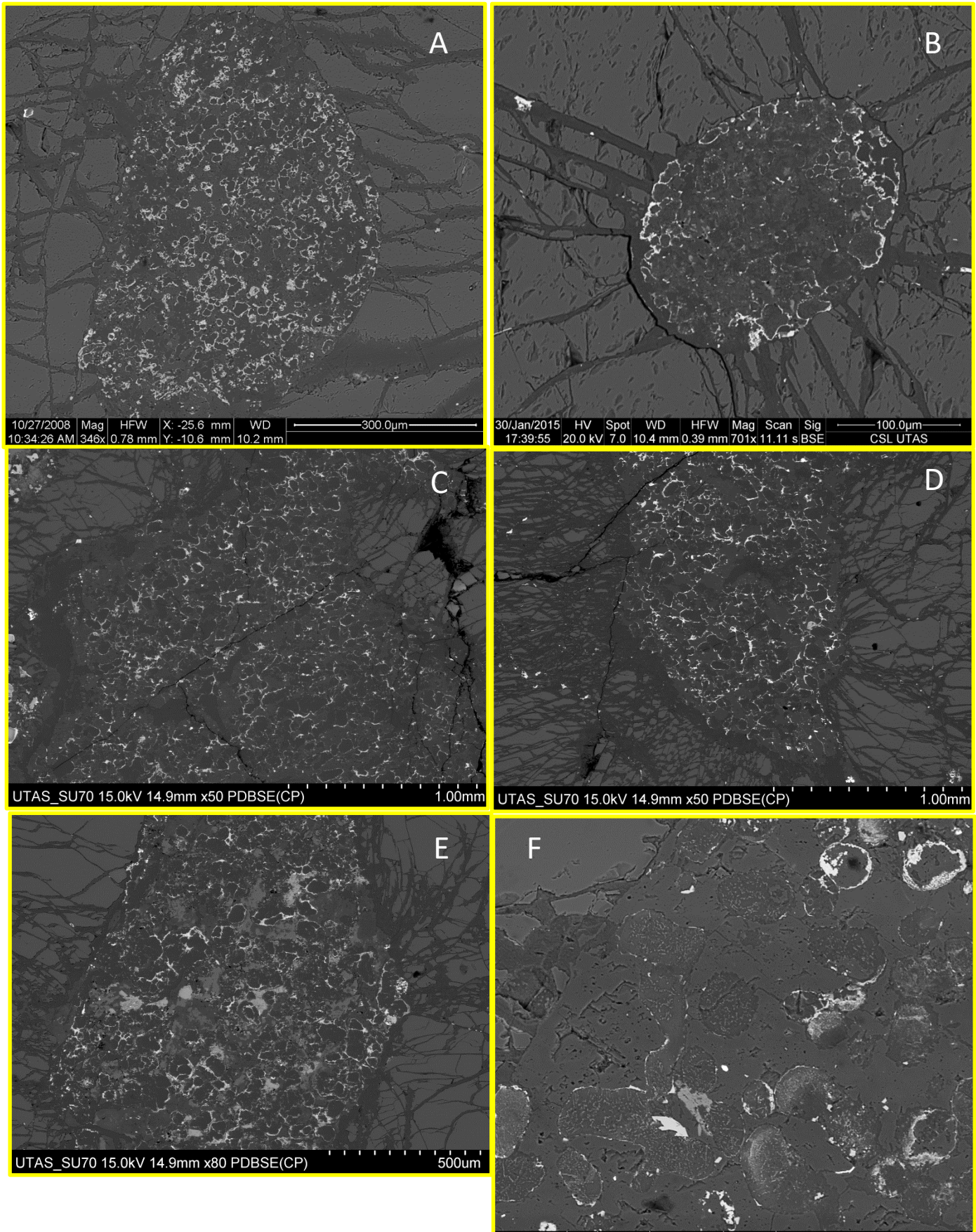


Figure S4. Inclusions (apatite, burbankite, halite, sylvite, djerfisherite, Na-bearing calcite) in dolomite and calcite from melt pools

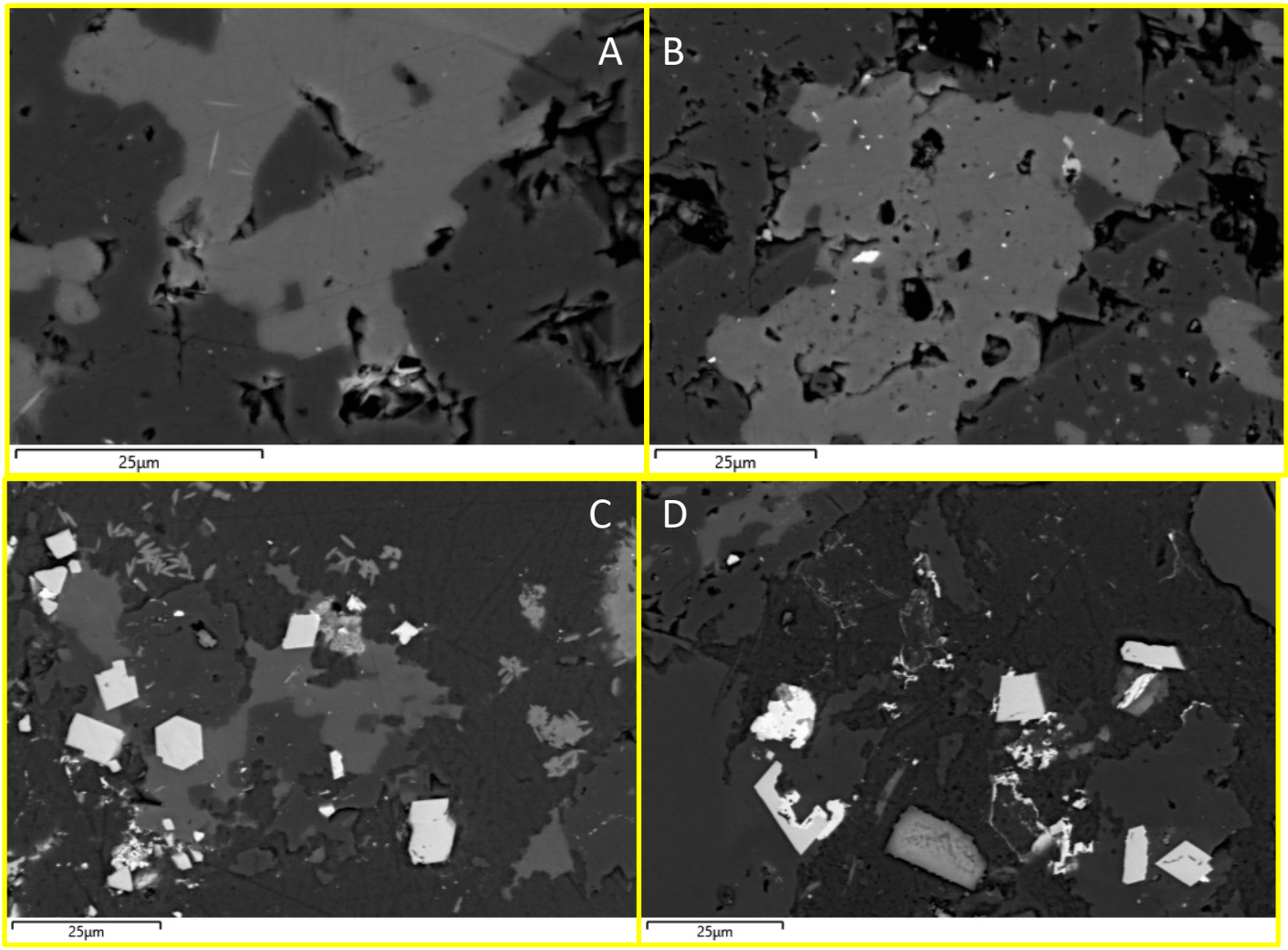


Figure S5 Zoned euhedral spinel with primary melt and crystal (periclase), aligned with growth zones

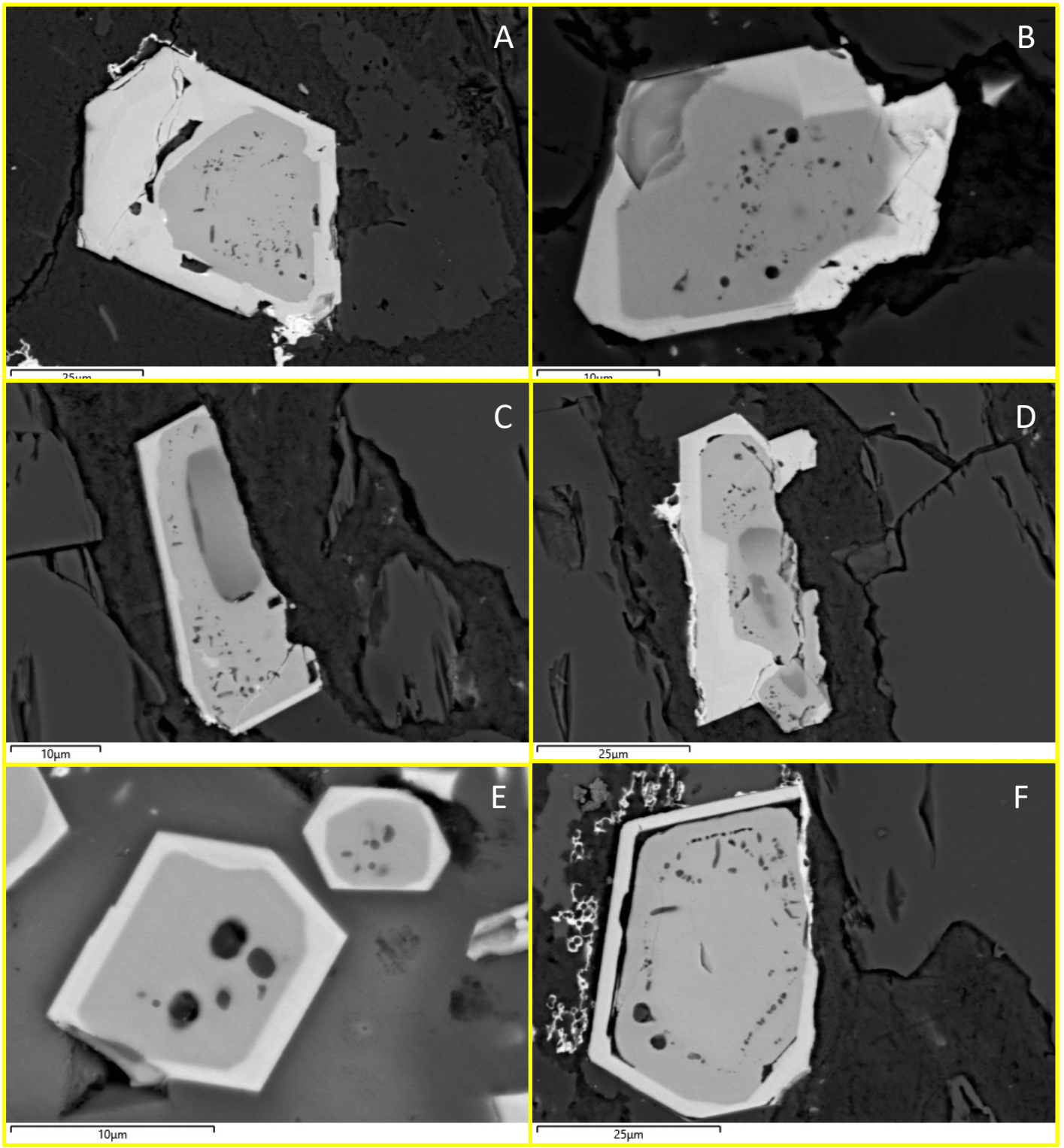
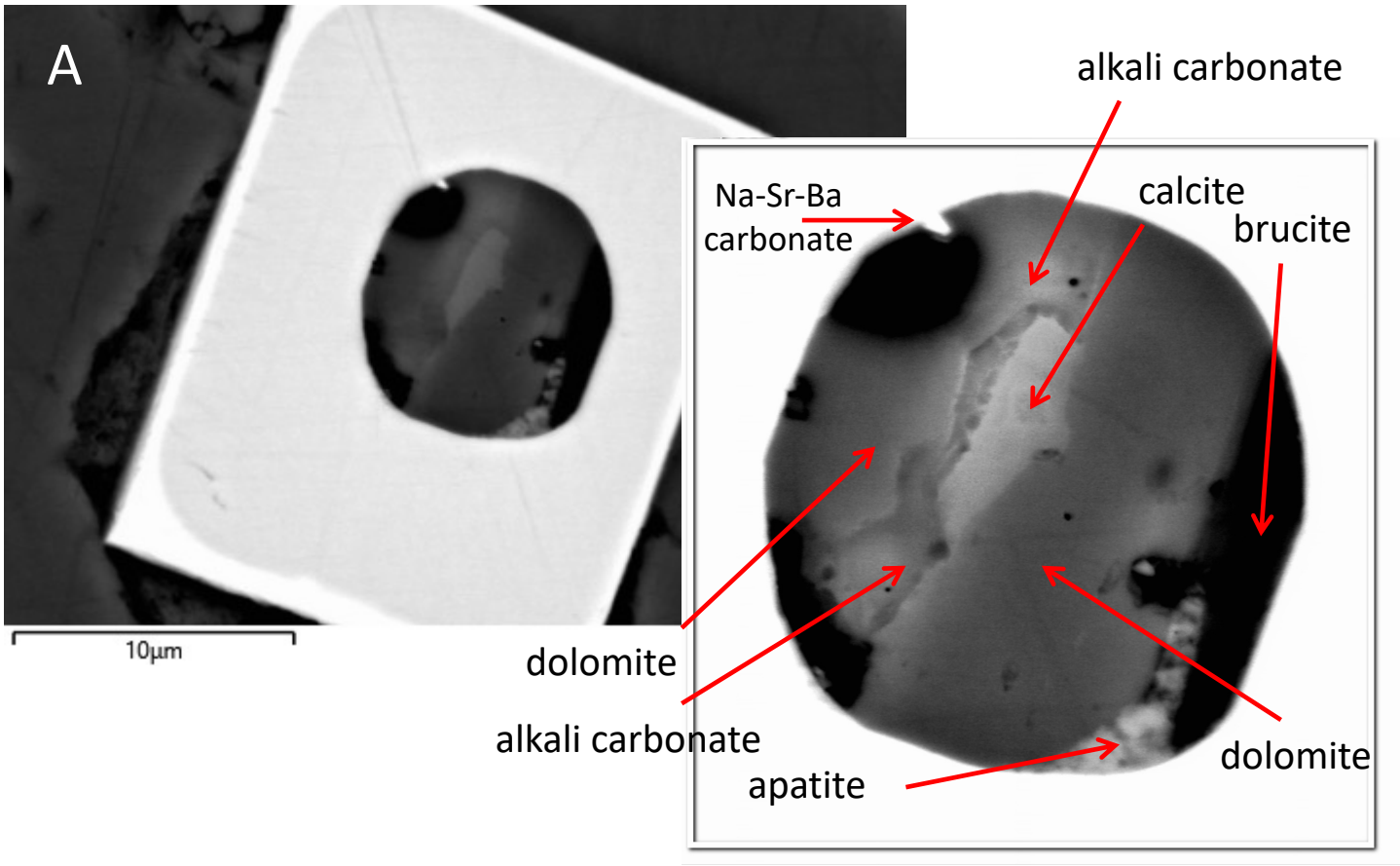
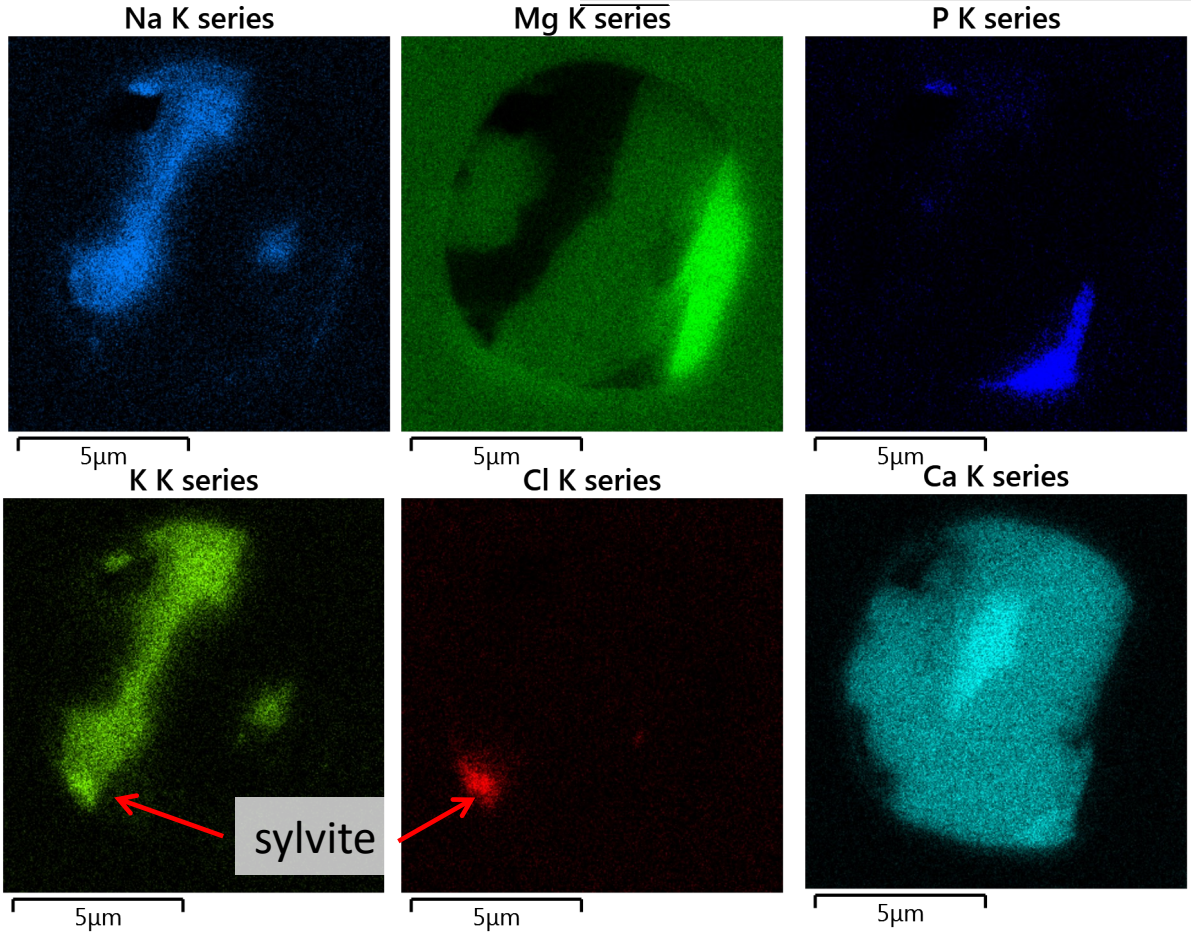
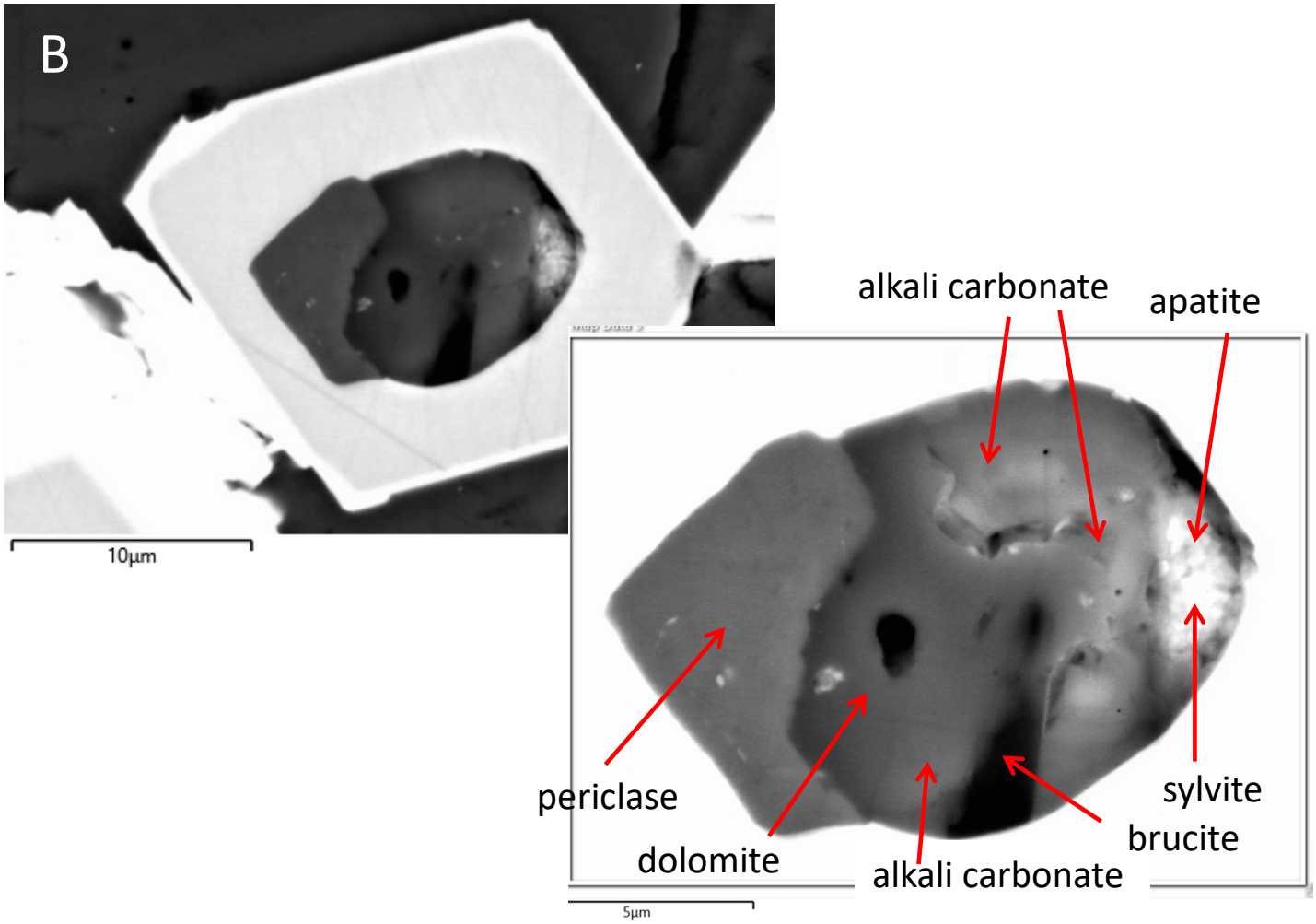
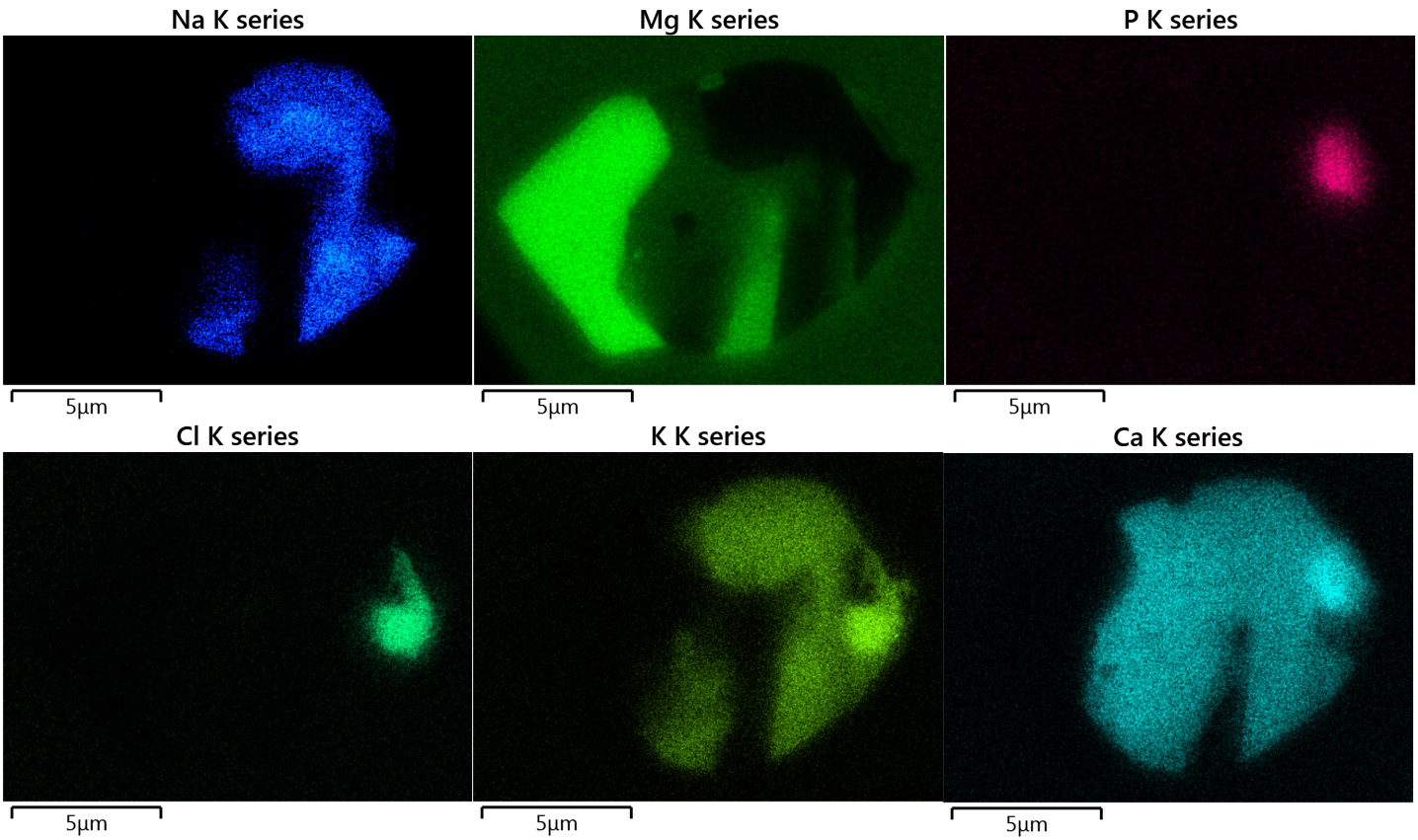


Figure S6. Backscattered electron images and EDS X-ray element maps of the exposed melt inclusions in the cores of euhedral spinel from the melt pools in wehrlite.

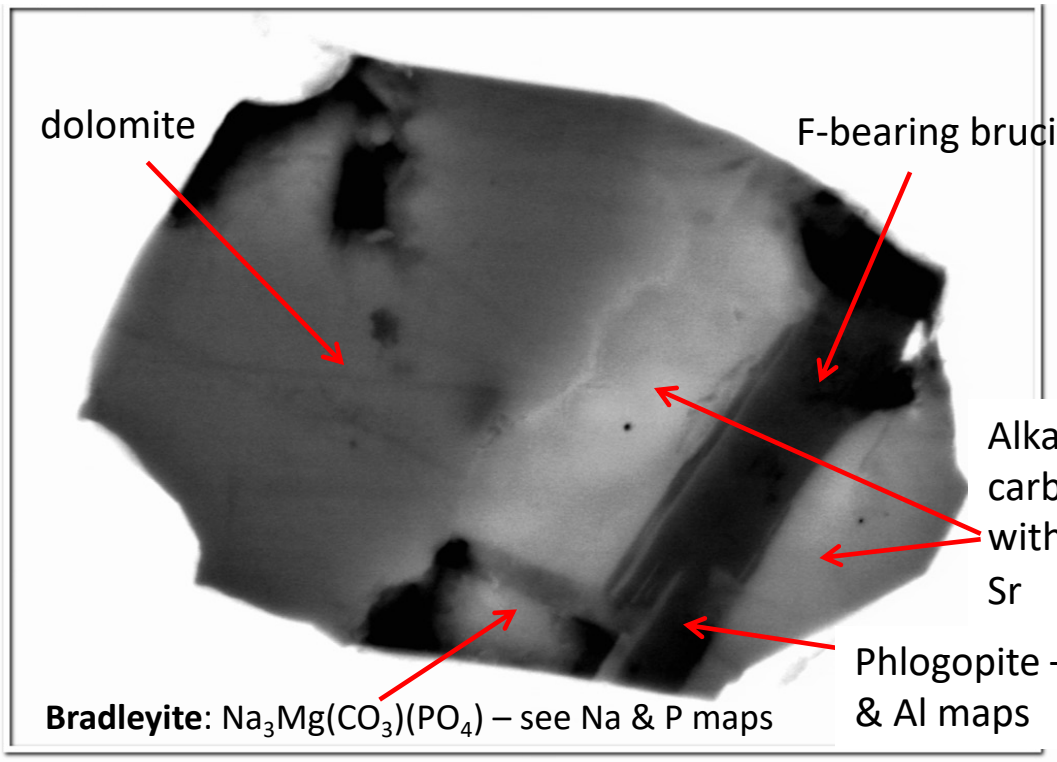


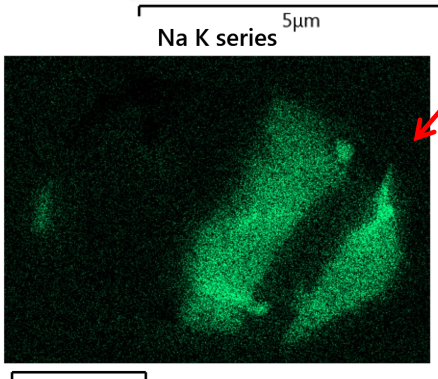


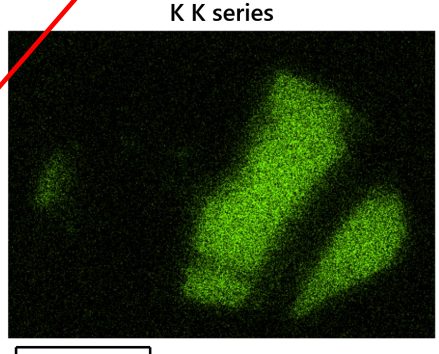

B
10μm
alkali carbonate
apatite
periclase
dolomite
alkali carbonate
sylvite
brucite
5μm

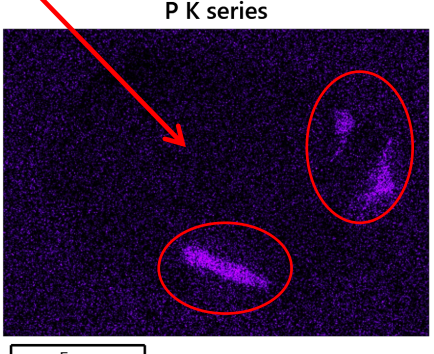

Na K series
Mg K series
P K series
5μm
5μm
5μm
Cl K series
K K series
Ca K series
5μm
5μm
5μm

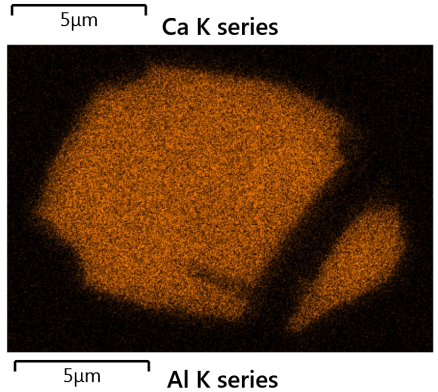
C

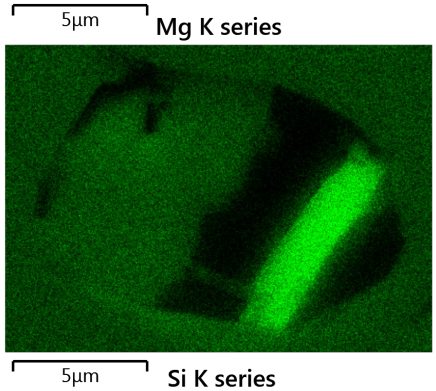

dolomite
F-bearing brucite
Alkali carbonate with Ba and Sr
Phlogopite – see Si & Al maps
Bradleyite: $Na_3Mg(CO_3)(PO_4)$ – see Na & P maps

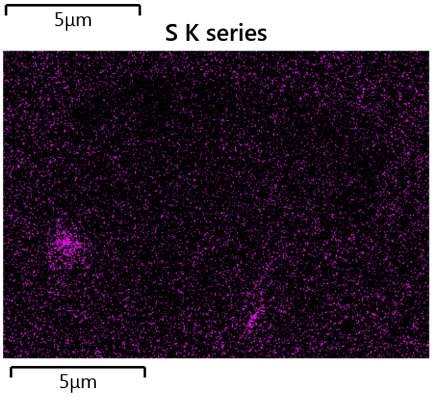

5µm
Na K series

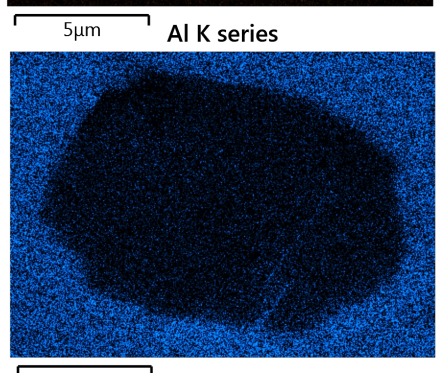

K K series
5µm

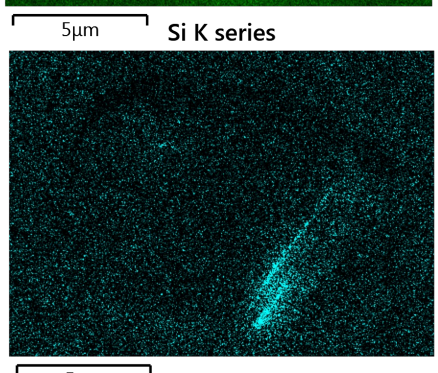

P K series
5µm


5µm
Ca K series

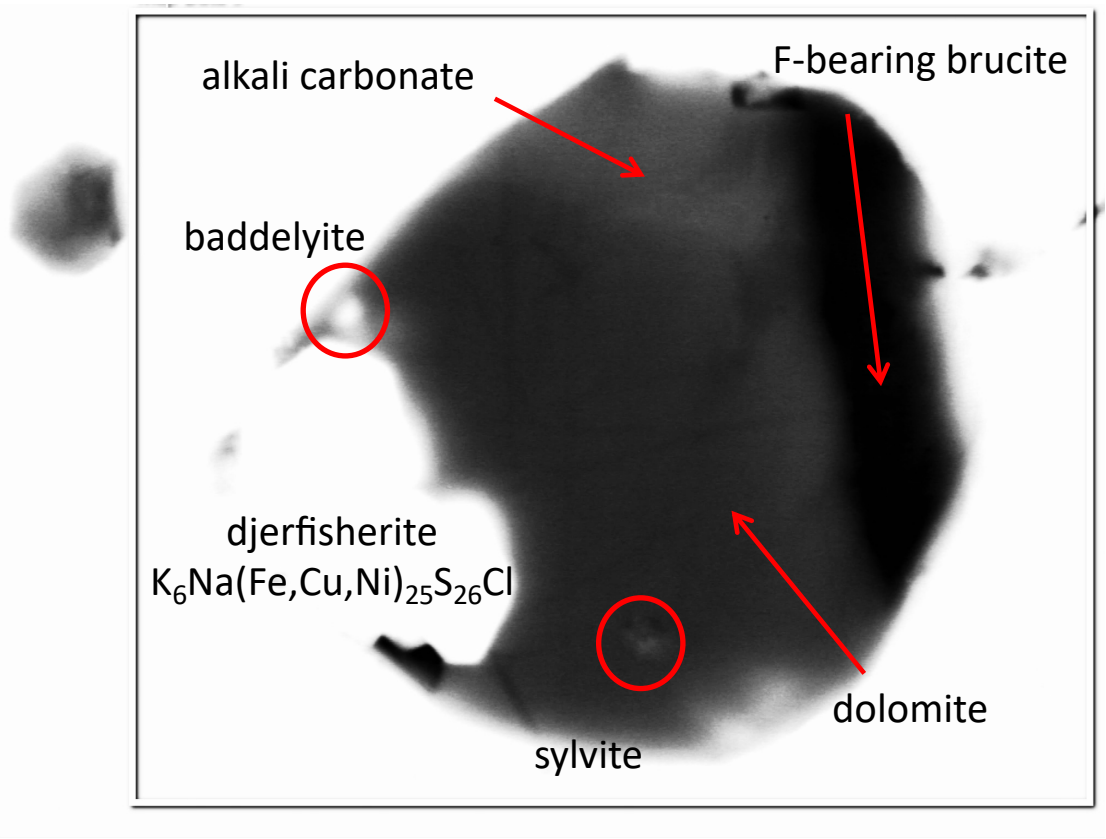

5µm
Mg K series

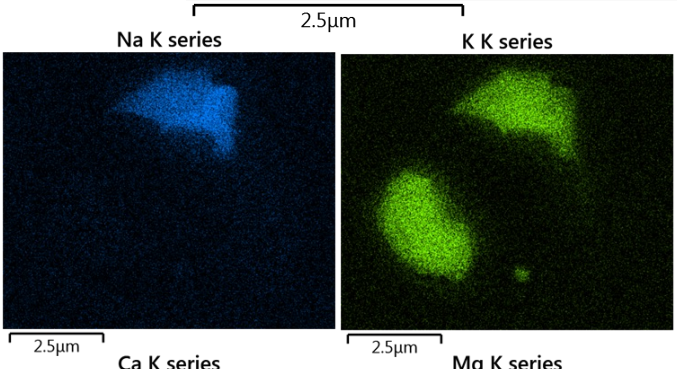

S K series
5µm


5µm
Al K series

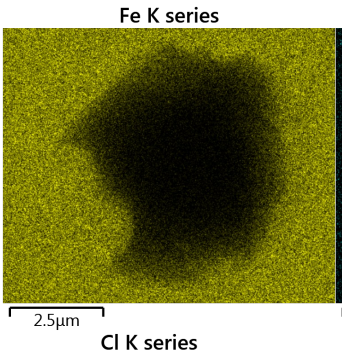

5µm
Si K series

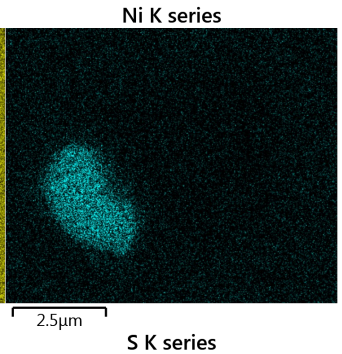
D

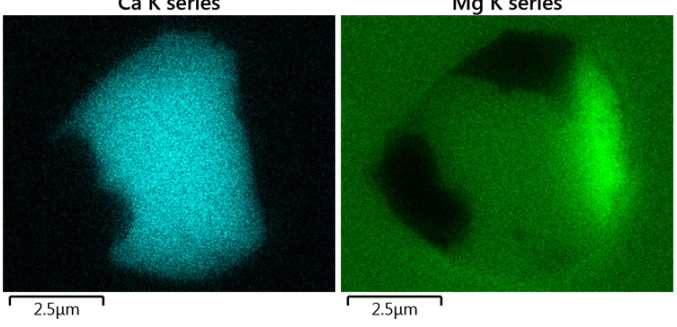

alkali carbonate
F-bearing brucite
baddelyite
djerfisherite
$K_6Na(Fe,Cu,Ni)_{25}S_{26}Cl$
dolomite
sylvite
2.5µm


Na K series
2.5µm

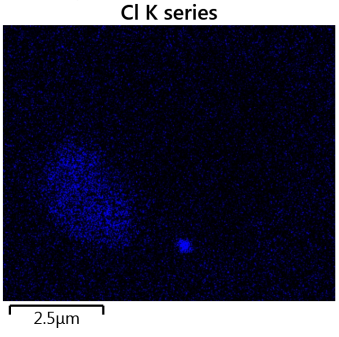
K K series
2.5µm

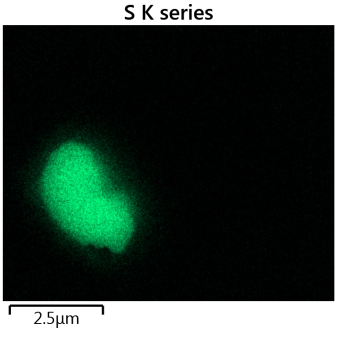

Fe K series
2.5µm


Ni K series
2.5µm

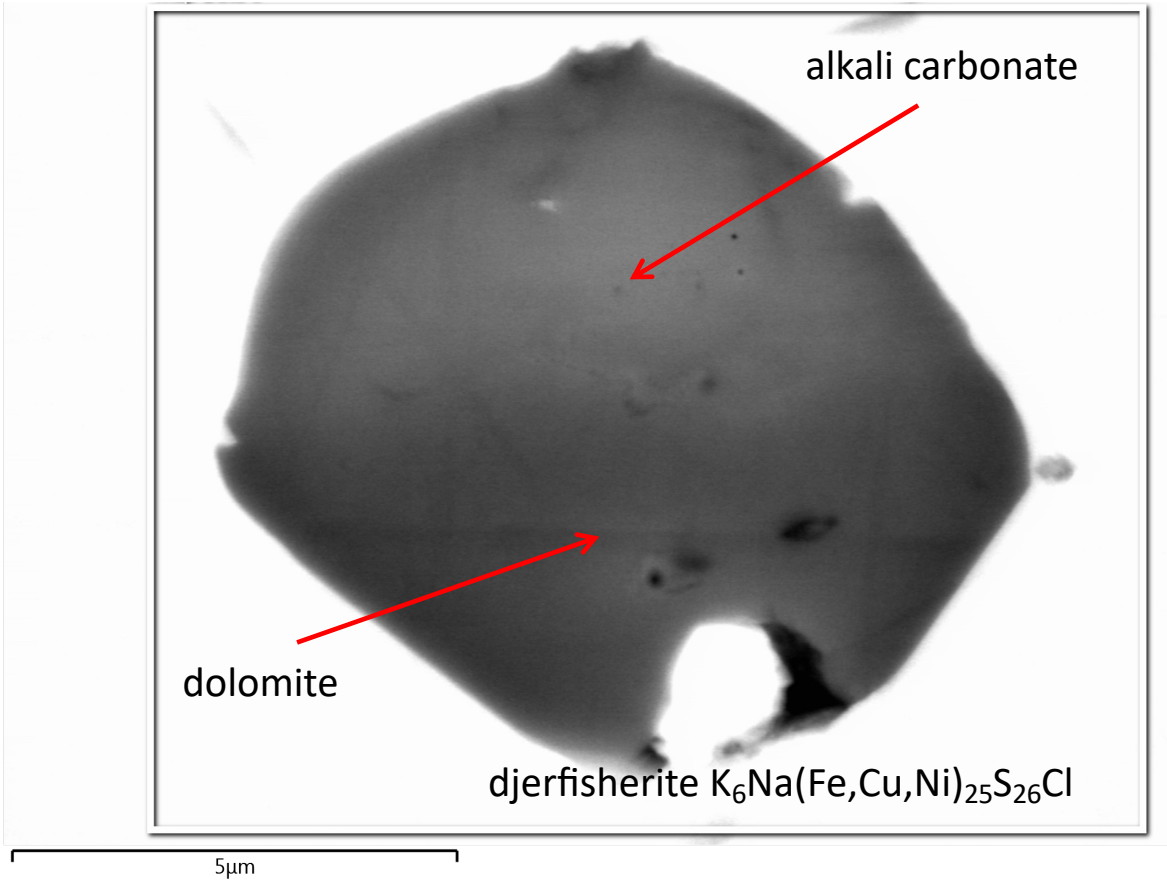

Ca K series
2.5µm

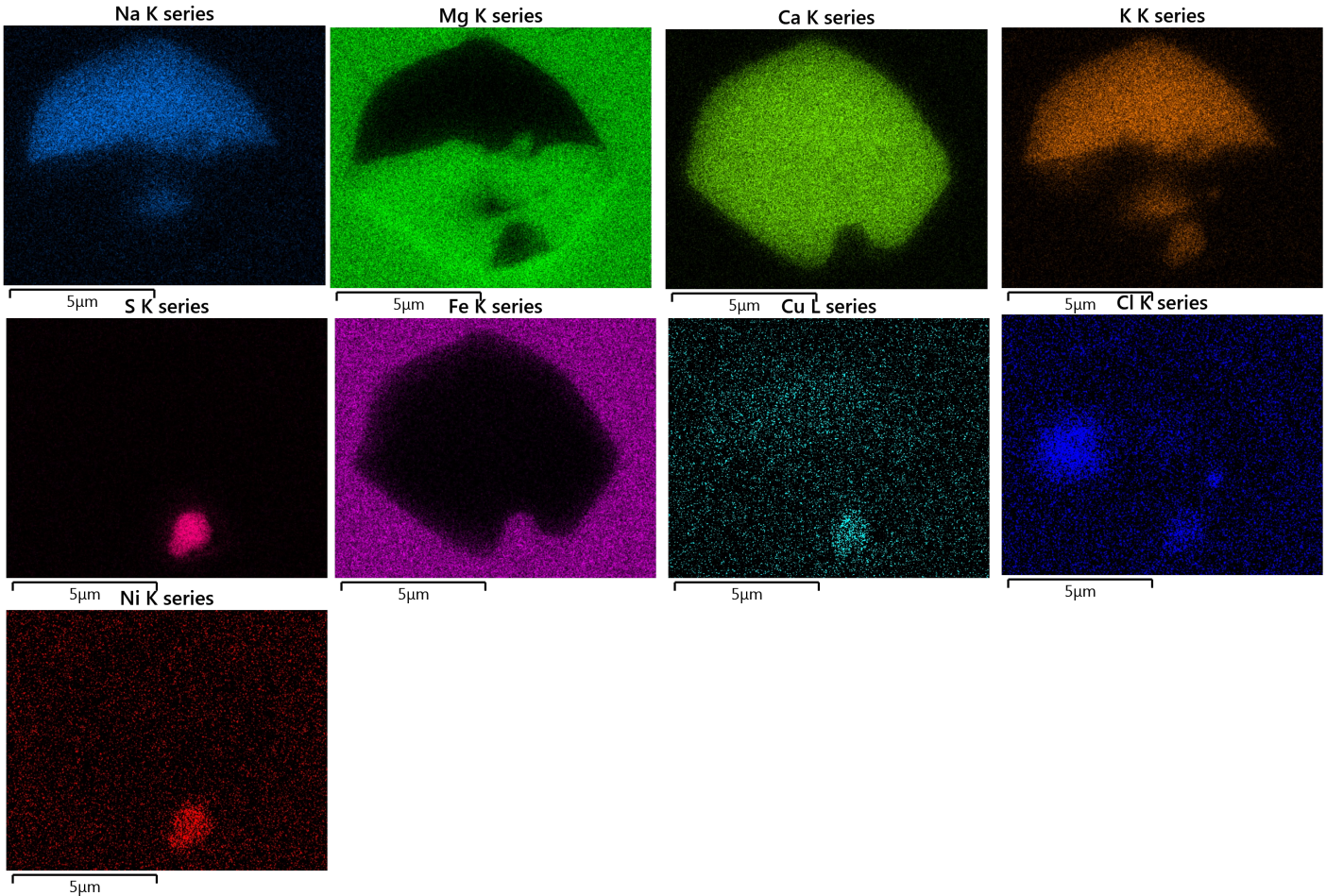
Mg K series
2.5µm


Cl K series
2.5µm


S K series
2.5µm

E


alkali carbonate
dolomite
djerfisherite $K_6Na(Fe,Cu,Ni)_{25}S_{26}Cl$
5µm


Na K series
5µm
Mg K series
5µm
Ca K series
5µm
K K series
5µm
S K series
5µm
Fe K series
5µm
Cu L series
5µm
Cl K series
5µm
Ni K series
5µm